Nano Research

Open Access

Research Article

New deltahedral architectures of rhodium-mediated Pn_7^{3-} (Pn = Sb and Bi) cages

Lei Qiao, Chuan-Ling Chen, and Zhong-Ming Sun ✉

State Key Laboratory of Element-Organic Chemistry, Tianjin Key Lab for Institution Rare Earth Materials and Applications, School of Materials Science and Engineering, Nankai University, Tianjin 300350, China

Cite this article: *Nano Research*, **2025**, *18*, 94907253. https://doi.org/10.26599/NR.2025.94907253

ABSTRACT: The reactions of K_5Pn_4 (Pn = Sb and Bi) and $CpRh(PPh_3)_2$ (Cp = C_5H_5, cyclopentadiene) in ethylenediamine (en) solutions resulted in a series of new Pn_7^{3-} adducts, $\{Pn_8[Rh(PPh_3)]_2\}^{2-}$, $\{Sb_7[Rh(PPh_3)]_2\}^{2-}$, and $\{Sb_7[Rh(PPh_3)]_3\}^{2-}$, through slight variations in reaction conditions. These clusters represent rare electron-deficient group 15 polyhedral clusters comprising Pn_7^{3-} with $RhPPh_3$ units in an η^5 coordination mode. Notably, the anionic clusters $\{Sb_8[Rh(PPh_3)]_2\}^{2-}$, $\{Sb_7[Rh(PPh_3)]_2\}^{2-}$, and $\{Sb_7[Rh(PPh_3)]_3\}^{2-}$ are the first Rh-Sb binary Zintl clusters to date. The synthesis, structure, and bonding of these new deltahedral hybrids were studied for the first time, revealing a highly versatile chemistry associated with classical Pn_7^{3-} cages and offering a pathway to prepare polyhedral hybrid clusters based on Pn_7^{3-} cages.

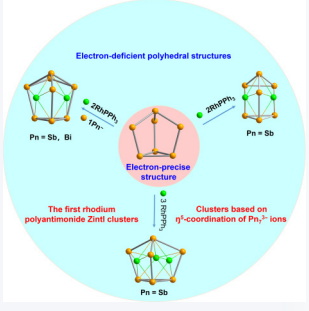

KEYWORDS: group 15 clusters, heterometallic clusters, nanoclusters-based materials, electronic structures, coordination modes

1 Introduction

Over the past few decades, Zintl ions and clusters have attracted extensive attention among scientists in inorganic and structural chemistry due to their diverse coordination modes, unique bonding situations and potential applications in nanoclusters-based materials [1–3]. One direction of this research activity is the construction of heterometallic clusters, $[M_xE_y]^{q-}$ (M = transition metals, E = main group elements), where the composition, proportion, and coordination modes of transition metals with main group elements in those clusters could provide important molecular-level insights into the formation process of (multi)metallic nanoparticles (NPs) [4]. Group 15 polyanions of P, As, Sb, and Bi with polycyclic hydrocarbon-like structures, which are important precursors in the synthesis of Zintl clusters, can react with transition metal complexes to afford heterometallic clusters with diverse structures [5–7]. The evolution of the electronic structure and topology of these heterometallic clusters provides valuable insight into the formation of group 15 bimetallic nanoparticles. As one of the most commonly used group 15 polyanions, heterometallic clusters based on nortricyclane-like Pn_7^{3-} (Pn = P, As, and Sb) anions have been extensively reviewed in the literature.

Received: November 21, 2024; **Revised:** January 1, 2025
Accepted: January 13, 2025

✉Address correspondence to sunlab@nankai.edu.cn

The related clusters are classified into the following four categories based on their coordination modes and electronic structures. The simplest mode is the η^1-coordination mode (Scheme 1(a)) [8], where the two-connected, formally negatively charged atoms of Pn_7^{3-} anions can coordinate a transition metal fragment. For example, von Schnering and coworkers reported a rare case, $[\eta^1\text{-}P_7\{FeCp(CO)_2\}_3]$ (Cp = C_5H_5, cyclopentadiene), in which three $CpFe(CO)_2$ units connect with three two-coordinate vertexes of the P_7^{3-} cage [9]. In addition to the η^1-like mode, the most common coordination modes available to Pn_7^{3-} anions are η^2 and η^4, in which they sever as four-electron and six-electron donors, respectively. In the former case, the η^2-coordination style does not change the nortricyclane-type architecture of the Pn_7^{3-} anions. One such example is $[M(\eta^2\text{-}Pn_7)_2]^{4-}$ (Pn = P, M = Zn and Cd; Pn = As, M = Zn) clusters (Scheme 1(b)), which are generally synthesized through the reaction of Pn_7^{3-} with MPh_2 compounds in ethylenediamine (en) [10–14]. In the η^4-coordination fashion, two twofold-bound atoms and two basal atoms of Pn_7^{3-} anions act as six-electron donors to coordinate highly unsaturated transition metal centers (Scheme 1(c)), leading to a structural transformation from the nortricyclane-type into a norbornadiene-like cage [15–17]. For example, Sb_7^{3-} anions substitute the 6-electron mesitylene ligand of $Cr(CO)_3(mes)$ (mes = mesitylene) to yield the $[\eta^4\text{-}Sb_7Cr(CO)_3]^{3-}$ cluster. Recently, Xu's group reported $[Bi_7M_3(CO)_3]^{2-}$ (M = Co and Rh) clusters (Scheme 1(d)), where three MCO units insert into the central site of each five-membered ring of the significantly expanded Bi_7^{3-} cage, forming an η^5-coordination mode [18]. These

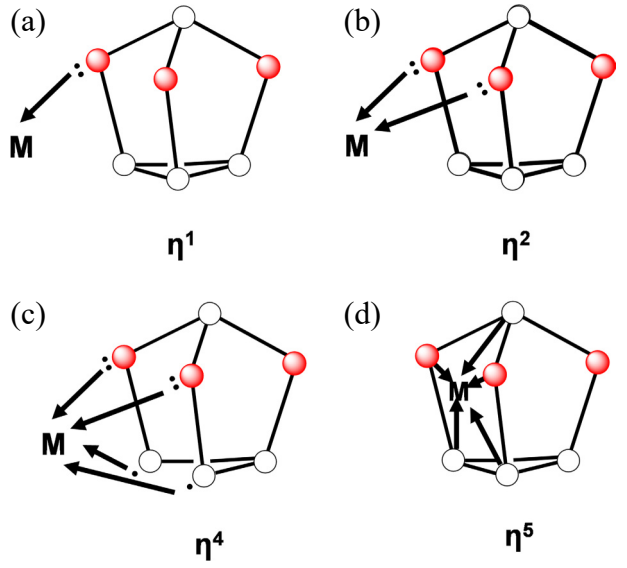

Scheme 1 Diagram showing the four known bonding modes of Pn_7^{3-}.

clusters represent the first examples of polyhedral polypnictogen hybrids with deltahedral faces through the coordination of Bi_5 rings with multimetallic fragments. However, significant challenges remain in the study of polypnictogen hybrids based on the η^5 coordination manner of Pn_7^{3-} anions: (1) only one $[Bi_7M_3(CO)_3]^{2-}$ (M = Co and Rh) cluster exhibiting the η^5 mode has been reported, with no novel structures or polyantimony compounds documented; (2) a comprehensive study on the syntheses and bonding of these clusters is still lacking. In this study, we present the syntheses, structural evolution, and bonding of a series of Pn_7^{3-} (Pn = Sb and Bi) adducts, including $\{Bi_8[Rh(PPh_3)]_2\}^{2-}$, $\{Sb_{7.13}[Rh(PPh_3)]_2\}^{2-}$ and $\{Sb_7[Rh(PPh_3)]_3\}^{2-}$, which could shed light on the formation mechanism of the new archetype of clusters based on the polycyclic η^5-coordination addition of Pn_7^{3-}. Notably, clusters $\{Sb_{7.13}[Rh(PPh_3)]_2\}^{2-}$ and $\{Sb_7[Rh(PPh_3)]_3\}^{2-}$ are also the first examples of rhodium polyantimonide Zintl clusters.

2 Experimental

2.1 Materials

Ethylenediamine (Aldrich, 99%), toluene (tol, Aldrich, 99.8%) and tetrahydrofuran (THF, 98%) were freshly distilled with sodium/benzophenone under a N_2 atmosphere and stored in N_2 prior to use. 2.2.2-Crypt (4,7,13,16,21,24-hexaoxa-1,10-diazabicyclo (8.8.8) hexacosane, purchased from Sigma-Aldrich, 98%) was dried under vacuum for one day before use. K_5Bi_4 and K_5Sb_4 were synthesized by heating a stoichiometric mixture of the elements at 600 °C for two days in a niobium tube [19]. $CpRh(PPh_3)_2$ was prepared according to the literature methodology [20, 21].

2.2 Synthesis

$[K(2.2.2\text{-crypt})]_2\{Bi_8[Rh(PPh_3)]_2\}\cdot en$ (1). K_5Bi_4 (103.1 mg, 0.1 mmol) and 2.2.2-crypt (120 mg, 0.36 mmol) were dissolved in en (3 mL). 35 mg (0.05 mmol) of $CpRh(PPh_3)_2$ was dissolved in 1 mL of toluene. A yellow toluene solution was added dropwise to the en solution while stirring vigorously. The resulting brown solution was then heated at 50 °C for 4 h. The reaction mixture was subsequently centrifuged (5000 rpm) and filtered through glass wool, and transferred to a test tube, and then carefully layered with toluene (4 mL). After 10 days, dark plate-shaped crystals of $[K(2.2.2\text{-crypt})]_2\{Bi_8[Rh(PPh_3)]_2\}\cdot en$ were obtained at a yield of 21% based on the precursor K_5Bi_4.

$[K(2.2.2\text{-crypt})]_2\{Sb_7[Rh(PPh_3)]_2\}_{0.87}\{Sb_8[Rh(PPh_3)]_2\}_{0.13}\cdot 2tol$ (2). A total of 55.4 mg (0.08 mmol) of $CpRh(PPh_3)_2$ was dissolved in 1 mL of THF to yield a yellow solution, which was added dropwise to an en solution of K_5Sb_4 (68.4 mg, 0.1 mmol) and 2.2.2-crypt (120 mg, 0.36 mmol). The resulting red-brown solution was then heated at 70 °C for 4 h. The reaction mixture was subsequently centrifuged (5000 rpm) and filtered through glass wool, transferred to a test tube, and then carefully layered with toluene (4 mL). After 7 days, dark block crystals were obtained at a yield of 23% based on the precursor K_5Sb_4.

$[K(2.2.2\text{-crypt})]_2\{Sb_7[Rh(PPh_3)]_3\}\cdot tol\cdot en$ (3). K_5Sb_4 (68.4 mg, 0.1 mmol) and 2.2.2-crypt (120 mg, 0.36 mmol) were dissolved in en (3 mL). In a second vial, 74 mg (0.11 mmol) $CpRh(PPh_3)_2$ was dissolved in 1 mL of toluene. A yellow toluene solution was added dropwise to the en solution while stirring vigorously. The resulting red-brown solution was then heated at 70 °C for 4 h. The reaction mixture was subsequently centrifuged (5000 rpm), and filtered through glass wool, transferred to a test tube, and then carefully layered with toluene (4 mL). After 10 days, dark block crystals of $[K(2.2.2\text{-crypt})]_2\{Sb_7[Rh(PPh_3)]_3\}\cdot tol\cdot en$ were obtained at a yield of 27% based on the precursor K_5Sb_4.

2.3 Characterizations

Suitable single crystals were selected for X-ray diffraction (XRD) analyses. Crystallographic data were collected on a Rigaku XtalAB Pro MM007 DW diffractometer with graphite monochromated Cu Kα radiation (λ = 1.54184 Å). The structures were solved via direct methods and then refined using SHELXL-2014 and Olex21-3 for convergence, in which all the nonhydrogen atoms were refined anisotropically during the final cycles [22–24]. All hydrogen atoms of the organic molecule were placed according to geometrical considerations and were added to the structure factor calculation. Negative ion mode electrospray ionization mass spectrometry (ESI-MS) of the acetonitrile solutions of the single crystals of compounds **1**, **2**, and **3** were measured on a linear trap quadrupole (LTQ) linear ion trap spectrometer by Agilent Technologies ESI-time-of-flight (TOF)-MS (6230). The spray voltage was 5.48 kV and the capillary temperature was maintained at 300 °C. Energy dispersive X-ray spectroscopy (EDS) analysis of compounds **1**, **2**, and **3** was performed using a field emission scanning electron microscopy (FE-SEM, JEOL JSM-7800F, Japan). Data acquisition was performed with an acceleration voltage of 15 kV and an accumulation time of 60 s.

2.4 Quantum chemical methods

All calculations described in this paper were performed with the Gaussian 09 software [25]. For all geometry optimizations, all PPh_3 groups in compounds **1**, **2**, and **3** were replaced by PMe_3 (denoted as $\mathbf{1}^{Me}$, $\mathbf{2}^{Me}$, and $\mathbf{3}^{Me}$) and a double-zeta quality basis set of Lanl2dz was used. All calculations adopted the generalized-gradient approximation (GGA) to the exchange potential, along with the exchange-correlation and gradient-corrected correlation functions of Perdew, Burke, and Ernzerhof (PBE0) [26]. The confining effect of cations in the solid-state was simulated by using a conductor polarizable continuum model (CPCM) with a dielectric constant of ε_r = 12.9. Chemical bonding analysis of compounds $\mathbf{1}^{Me}$, $\mathbf{2}^{Me}$, and $\mathbf{3}^{Me}$ was performed by the adaptive natural density partitioning

(AdNDP) method [27] at the same level of theory of structure optimization. The related calculations were analyzed by the Multiwfn 3.7 software [28].

3 Results and discussion

Compound **1** was prepared through the reaction between K_5Bi_4 and a toluene solution of $Rh(PPh_3)_2Cp$ at a ratio of 2:1 in ethylenediamine (Scheme 2). The resulting brown solution was stirred for 4 h at 50 °C, centrifuged, and carefully layered with toluene, yielding black block crystals with an approximate yield of 21% after 10 days. When Zintl alloy K_5Bi_4 was replaced with K_5Sb_4 and the stoichiometry ratio was changed from 2:1 to 5:4, a red-brown solution formed immediately. Upon heating the solution to 70 °C for 4 h, it was subsequently filtered and then layered with toluene, yielding irregular black crystals in 23% yield, accompanied by unknown black impurities (see Fig. S1 in the Electronic Supplementary Material (ESM)). Compound **3** was isolated in a manner similar to that used for the synthesis of compound **2**, except that a 1:1.1 ratio of the starting materials was used (Scheme 2).

Single-crystal XRD (SC-XRD) revealed that compounds **1** and **2** crystallize in the triclinic space group $P\bar{1}$. The asymmetric unit of compound **1** consists of one anionic cluster $\{Bi_8[Rh(PPh_3)]_2\}^{2-}$, two $[K(2.2.2\text{-crypt})]^+$ cations, and one en solvent molecule, whereas crystal **2** encountered severe disorder (Fig. S4 in the ESM). Hence, the composition of compound **2** was further characterized via electrospray ionization mass spectrometry. The presence of the monoanionic clusters $[Sb_7Rh_2(PPh_3)_2]^-$ and $\{[K(2.2.2\text{-crypt})][Sb_8Rh_2(PPh_3)_2O_4]^-$ (the overall charge state of Zintl clusters and their fragments are generally oxidized to −1 in the negative-ion mode ESI-MS in solution) confirmed that compound **2** contains a mixture of $\{Sb_7[Rh(PPh_3)]_2\}^{2-}$ and $\{Sb_8[Rh(PPh_3)]_2\}^{2-}$ (Fig. S8 in the ESM). The crystal data were refined to obtain an optimal model based on these two components, and compound **2** can be characterized as $[K(2.2.2\text{-crypt})]_2\{Sb_7[Rh(PPh_3)]_2\}_{0.87}\{Sb_8[Rh(PPh_3)]_2\}_{0.13}\cdot 2$ tol, as its asymmetric unit contains two $[K(2.2.2\text{-crypt})]^+$ cations, and two toluene molecules and one disordered cluster structure $\{Sb_7[Rh(PPh_3)]_2\}_{0.87}\{Sb_8[Rh(PPh_3)]_2\}_{0.13}^{2-}$. Notably, the cluster $\{Sb_8[Rh(PPh_3)]_2\}^{2-}$ is isomorphic to $\{Bi_8[Rh(PPh_3)]_2\}^{2-}$.

The anionic clusters $\{Pn_8[Rh(PPh_3)]_2\}^{2-}$ (Pn = Sb and Bi), as shown in Fig. 1, can be viewed as 10-vertex hybrid clusters composed of Pn_7^{3-} (Pn = Sb and Bi), which adopt a nortricyclane-type structure comprising one apical Pn1, three linking atoms (Pn2, Pn3, Pn4) and three basal atoms (Pn5, Pn6, Pn7), along with two $RhPPh_3$ fragments and a Pn8 atom. The latter two are coordinated to three five-membered rings of Pn_7^{3-} via the η^5 and η^2 modes, respectively. The Bi–Bi distances can be divided into three classes based on the coordination of Rh units. The first category includes Bi1–Bi3, Bi2–Bi5, Bi4–Bi7, and Bi5–Bi7, with the distances of 2.999, 3.050, 3.050, and 3.000 Å, respectively, in the Bi_7^{3-} cage [29], which falls within the typical range of Bi–Bi bonds. The second category includes Bi2–Bi8 and Bi4–Bi8, with distances of 2.947 and 2.935 Å, respectively, which are comparable to those in the first category but shorter than those found in clusters such as $[Bi_3Cr_2(CO)_6]^{3-}$, $[Bi_3Ni_4(CO)_6]^{3-}$ and $[Ga@Bi_{10}(NbMes)_2]^{3-}$ [30–32]. The remaining Bi–Bi distances are longer than the Bi–Bi bond length in Bi_7^{3-}, 3.15 Å, and comparable to those in $[Bi_6Mo_3(CO)_9]^{4-}$ and $[Bi_9\{Ru(cod)\}_2]^{3-}$ (cod = 1,5-cyclooctadiene), indicating the presence of the delocalized bonding [33, 34]. The Rh–Bi bond lengths of 2.696–2.835 Å are comparable to those in $[Bi_7(RhCO)_3]^{2-}$ (av. 2.770 Å) and the μ^3-Bi–Rh distances in $[Bi@Rh_{14}(CO)_{27}Bi_2]^{3-}$ (2.724–2.784 Å) [35], suggesting covalent interactions featuring $RhBi_2$ three-center–two-electron (3c–2e) bonds within this cluster. The Rh–Rh distance (2.855 Å) is longer than the sum of the atomic radius (2.70 Å) [36] but shorter than the reported distance in the cluster $[Bi_7(RhCO)_3]^{2-}$ (3.009 Å), indicating weak bonding interactions. The structure of cluster $\{Sb_8[Rh(PPh_3)]_2\}^{2-}$ will not be discussed in detail as it is isomorphous to $\{Bi_8[Rh(PPh_3)]_2\}^{2-}$, and its X-ray diffraction data is hampered by disorder.

Cluster $[Sb_7Rh_2(PPh_3)_2]^{2-}$ has a norbornadiene-like structure that is coordinated with two $PhPPh_3$ fragments, which results in shorter contacts of Sb2–Sb4 and Sb5–Sb7. This coordination is markedly distinct from clusters $[Pn_7M(CO)_3]^{3-}$ (Pn = P, As, and Sb; M = Cr, Mo, and W), where an open Pn_7 cage is bound in an η^4 fashion to the $M(CO)_3$ fragment. As shown in Fig. 2, the bicyclic η^5-coordination addition of an Sb_7 framework, along with two $RhPPh_3$ units, occurs at each central site of the Sb_5^{5-}-like rings, which consists of one apical atom, two linking atoms, and two basal atoms. The two Rh atoms can also be viewed as two missing apexes of a 9-vertex "*nido*-type" cluster, reminiscent of the reported *nido*-type $[Sb_7Ni_3(CO)_3]^{3-}$ cluster obtained from Ni(CO) fragment-induced Sb_7^{3-} rearrangement [37]. The Sb1–Sb3, Sb5–Sb6, and Sb6–Sb7 separations of 3.1952, 3.1321, and 3.0887 Å, respectively, are significantly longer than those of Sb_7^{3-} (av. 2.78 Å) [38, 39], which are predominantly influenced by the coordination of Rh fragments. The remaining Sb–Sb distances in $[Sb_7Rh_2(PPh_3)_2]^{2-}$ (av. 2.902(1) Å) are slightly longer than those in Sb_7^{3-} (2.70 Å). The Rh–Sb bond lengths lie in a range of 2.642–2.726 Å, which is shorter than those bond involving the peripheral Rh atoms with the interstitial Sb atoms (average value of 2.800(13) Å) in transition-

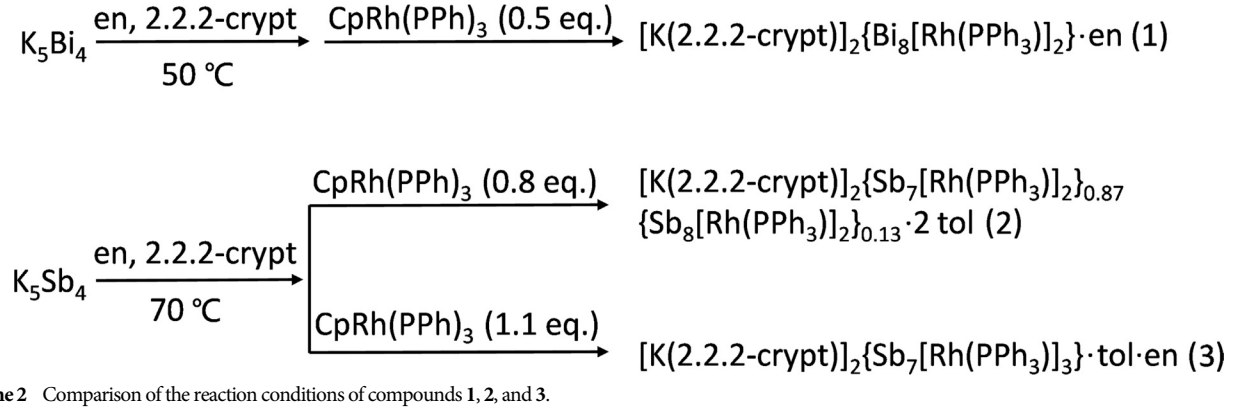

Scheme 2 Comparison of the reaction conditions of compounds **1**, **2**, and **3**.

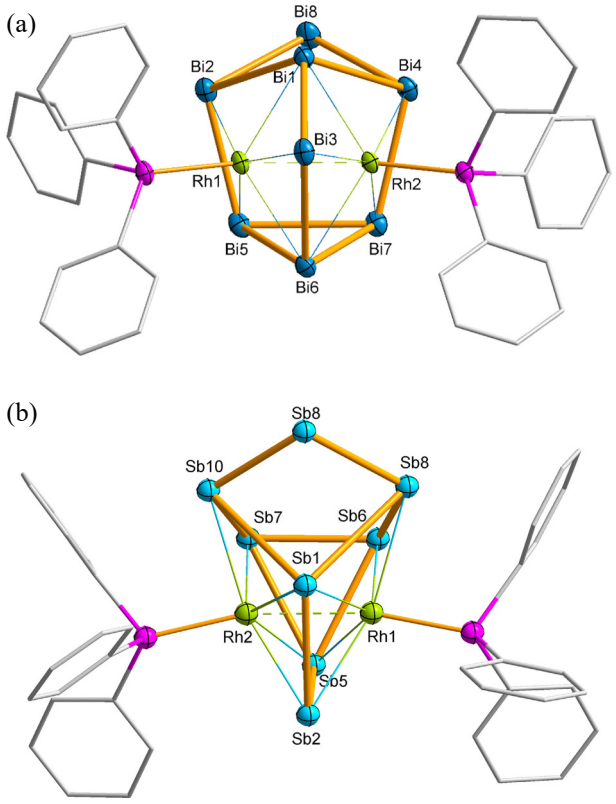

Figure 1 Thermal ellipsoid plots of clusters (a) $\{Bi_8[Rh(PPh_3)]_2\}^{2-}$ and (b) $\{Sb_8[Rh(PPh_3)]_2\}^{2-}$ (drawn at 50% probability).

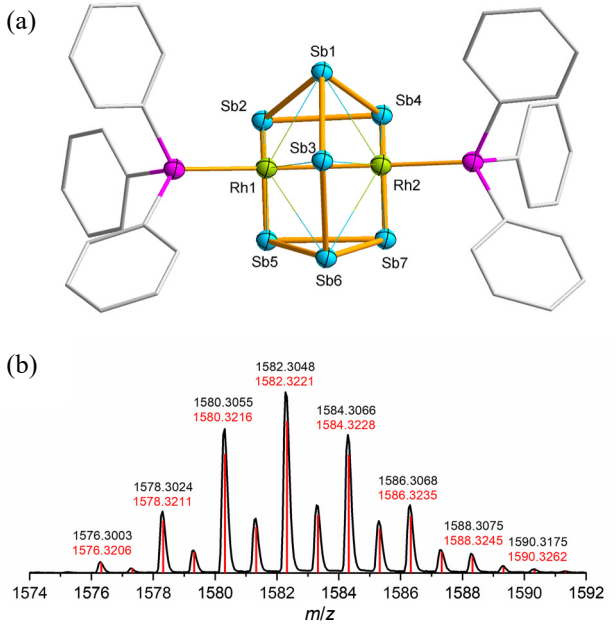

Figure 2 (a) Thermal ellipsoid plots of cluster $\{Sb_7[Rh(PPh_3)]_2\}^{2-}$ (drawn at 50% probability). (b) ESI(−) mass peak corresponding to $\{Sb_7[Rh(PPh_3)]_2\}^-$. The experimental mass distributions are depicted in black, and the theoretical masses of the isotope distributions are shown in red.

metal carbonyl clusters $[Rh_{20}Sb_3(CO)_{36}]^{3-}$ but comparable to those in $[Rh_{21}Sb_2(CO)_{38}]^{5-}$ (average value of 2.7265(9) Å). and are shorter than the sum of their atomic radii (Rh–Sb, 2.80 Å) [40].

SC-XRD analysis of compound **3** revealed that it crystallizes in the monoclinic space group $P2_1/n$. The asymmetric unit of compound **3** consists of one anionic cluster, two $[K(2.2.2\text{-crypt})]^+$ cations, one en molecule and one tol molecule. The anionic cluster $\{Sb_7[Rh(PPh_3)]_3\}^{2-}$ is a 10-vertex deltahedral cluster built from an Sb_7^{3-} cage and three $RhPPh_3$ fragments, as shown in Fig. 3. The apical-linking Sb–Sb contacts (3.179, 3.148, and 3.308 Å) and the triangular basal separations (3.288, 3.283, and 3.337 Å) in $\{Sb_7[Rh(PPh_3)]_3\}^{2-}$ are significantly longer than those in Sb_7^{3-} and Sb_{11}^{3-} [41, 42], indicating that covalent interactions involve $RhSb_2$ 3c–2e bonds. The linking-basal distances in $\{Sb_7[Rh(PPh_3)]_3\}^{2-}$ (2.811, 2.834, and 2.797 Å) are largely consistent with those in classical Sb_7^{3-} and Sb_{11}^{3-}. The Rh–Rh contacts (3.065, 3.032, and 3.069 Å) are minimally influenced by the type of Pn_7^{3-} and are consistent with those in $\{Bi_7[Rh(CO)]_3\}^{2-}$ (av. 3.009 Å). All Rh–Sb bonds in the $\{Sb_7[Rh(PPh_3)]_3\}^{2-}$ cluster are between 2.636 and 2.738 Å, comparable to those in the $[Sb_7Rh_2(PPh_3)_2]^{2-}$ cluster, and are both muti-center two-electron bonds.

Cluster $\{Bi_8[Rh(PPh_3)]_2\}^{2-}$ shows both electron-precise structural motifs common to polypnictides and delocalized-bonding deltahedral fragments, thus making it challenging to explain the bonding of the cluster using Wade–Mingos rules [43] or the polyhedral skeletal electron pair theory (PSEPT) [44, 45]. Therefore, we employed quantum-chemical studies to investigate the bonding within the target cluster. The optimized structure of cluster $\{Bi_8[Rh(PMe_3)]_2\}^{2-}$ (where the phenyl substituents were replaced by methyl units, such a treatment that does not affect the bonding of the cluster.) shows a good correlation with its crystal structure. The errors in the optimized Bi–Bi, Rh–Bi, and Rh–Rh distances are within 5% of the experimental values, so it is clear that the computational model captures the essential geometric features of the cluster. To further elucidate the bonding characteristics of the title clusters, adaptive natural density partitioning analysis was performed by using the Multiwfn 3.7 program. Since clusters $\{Bi_8[Rh(PPh_3)]_2\}^{2-}$ and $\{Sb_8[Rh(PPh_3)]_2\}^{2-}$ share similar bonding characteristics, we analyzed the bonding picture of cluster $\{Bi_8[Rh(PMe_3)]_2\}^{2-}$ as a representative example. The computational details of the quantum chemical calculations are provided in the ESM. The cluster model contains 112 valence electrons, which can be partitioned into 56 two-electron bonding elements. We initiated the localization procedure with one-center–two-electron (1c–2e) elements (lone pairs, LPs), including four d-type lone pairs on each Rh atom with occupation numbers (ONs) between 1.94 and 1.80|e| (Fig. S23(a) in the ESM) and eight s-type lone pairs on Bi atoms

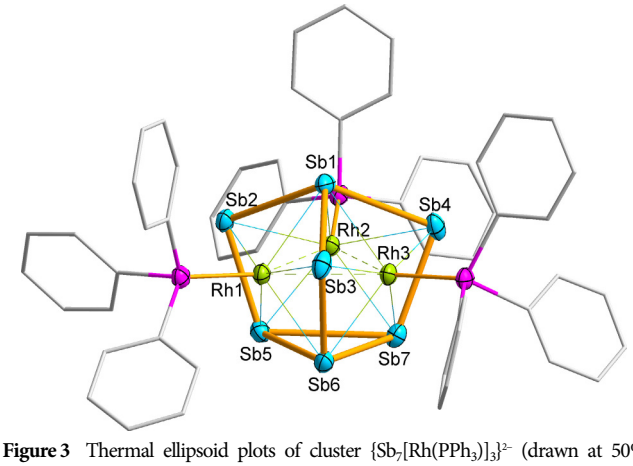

Figure 3 Thermal ellipsoid plots of cluster $\{Sb_7[Rh(PPh_3)]_3\}^{2-}$ (drawn at 50% probability).

with ONs = 1.97–1.91|e| (Fig. 4(a)). The chemical bonding within the PMe_3 ligands consists of six two-center two-electron (2c–2e) C–P σ bonds and eighteen 2c–2e C–H σ bonds (Figs. S23(b) and S23(c) in the ESM). The binding interactions between the PMe_3 fragment and the metal cluster are facilitated through one 2c–2e P–Rh bond with ON = 1.96|e| (Fig. 4(c)). Six classical 2c–2e Bi–Bi bonds (ON = 1.96–1.78|e|) are responsible for the direct bonding between Bi atoms constituting the framework of the cluster (Fig. 4(b)). In addition to the abovementioned bonding elements, the remaining 16 electrons on the 10-vertex hybrid cluster core can be localized into the following bonding types: the first type is one 3c–2e Bi–Bi–Bi bond with ON = 1.79|e| (Fig. 4(g)), which represents a linear combination of 6p orbitals of the Bi8 atom with 6p orbitals on two adjacent Bi atoms (Bi2 and Bi4), with the major contribution coming from Bi8 (90.67%, 4.55%, and 4.78% from Bi8, Bi2, and Bi4, respectively). Notably, the 3c–2e Bi–Bi–Bi bond can also be recovered as a pure p-type LP on the Bi8 atom with lower ON values, approximately 1.62|e|, and thus, the interaction is better described as a 3c–2e interaction. Similar bonding conditions were also found for clusters $[Au_2Sb_{16}]^{4-}$ and $[As_7Cu(PPh_3)]^{2-}$) [46]. The second type is six 3c–2e σ Rh–Bi–Bi bonds with ON values ranging from 1.87 to 1.71|e| (Figs. 4(d)–4(f)), attributed to interactions between the three elongated Bi–Bi bonds in the Bi_7^{3-} cage and the Rh atoms, which is reminiscent of the interactions between Sn cages with Ru atoms in $[Sn_{19}\{Ru(cod)(en)\}_2]^{4-}$ and $[Sn_{20}\{Ru(cod)\}_2]^{6-}$ [47]. The Rh d atomic orbitals (AOs) contribute up to 21.81%–29.75% of the formation of these 3c–2e σ bonds. Finally, a multi-center delocalized bond is identified around the two Rh atoms, as indicated by the residual density distributions within the cluster $\{Bi_8[Rh(PMe_3)]_2\}^{2-}$. Specifically, a five-center two-electron (5c–2e) σ bond is present in the Rh_2Bi_3 unit with ON = 1.70|e| (Fig. 4(h)). The contribution of two Rh atoms to the formation of this bond is assessed to be approximately 75.2%, which is consistent with the weak interactions of the two Rh atoms.

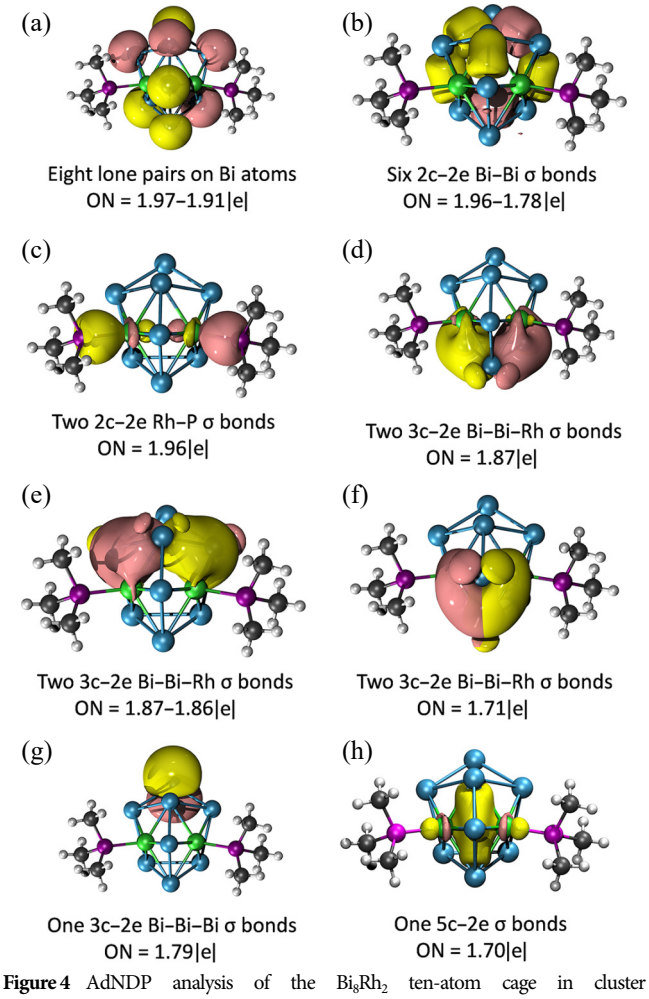

Figure 4 AdNDP analysis of the Bi_8Rh_2 ten-atom cage in cluster $\{Bi_8[Rh(PMe_3)]_2\}^{2-}$.

Cluster $\{Sb_7[Rh(PPh_3)]_2\}^{2-}$, containing an unpaired electron, exhibits a doublet ground state, as determined by density functional theory (DFT) calculations (see the ESM). All attempts to obtain the electronic paramagnetic resonance (EPR) spectra of compound **2** in either solution or solid-state were unsuccessful, likely because of its extreme air sensitivity and propensity for oxidation. DFT calculations were used to investigate the electron density distribution of cluster $\{Sb_7[Rh(PMe_3)]_2\}^{2-}$. The DFT-optimized structure of $\{Sb_7[Rh(PMe_3)]_2\}^{2-}$ closely resembles that obtained from the X-ray experiment, although errors in a few Sb–Sb bond lengths (0.1 Å) were observed. This discrepancy is a common observation in Zintl clusters, likely resulting from the absence of a cationic environment in the computational model [48–50]. DFT calculations revealed that cluster $\{Sb_7[Rh(PMe_3)]_2\}^{2-}$ contains 54α electrons and 53β electrons. Further calculations revealed that the singly occupied molecular orbital (SOMO) and electron spin density of the cluster (one α electron) are located primarily at the Sb2, Sb3, Sb4, and Sb6 atoms (Fig. S26 in the ESM and Fig. 5).

The remaining 106 valence electrons in cluster $\{Sb_7[Rh(PMe_3)]_2\}^{2-}$ can be partitioned into the following classes, excluding the d-type lone pairs on Rh atoms and classical 2c–2e bonds in three PMe_3 units (Fig. S24 in the ESM, four 1c–2e bonds on each Rh atom, eighteen 2c–2e C–H bonds, and six P–C bonds, with occupation numbers of 1.95–1.79|e|, 1.99|e|, and 1.98|e|, respectively). The first category is seven s-type lone pairs on each Sb atom with ONs = 1.94–1.92|e| (Fig. 6(a)). The second class consists of two 2c–2e Rh–P (Fig. 6(b)) and two 2c–2e Sb–Sb (Fig. 6(c)) bonds with ONs of 1.97 and 1.98–1.97|e|, respectively. The third category is ten 3c–2e Rh–Sb–Sb bonds (Fig. 6(d)), representing interactions between the Rh atom and the corresponding Sb atoms.

Cluster $\{Sb_7[Rh(PMe_3)]_3\}^{2-}$ is a 10-vertex deltahedral cluster that consists of fifteen Rh–Sb–Sb bonds and one Sb_3 triangle. The 70 cluster valence electrons (CVEs), provided by seven Sb atoms (7 × 5), three Rh atoms (3 × 9), three PMe_3 units (3 × 2) and two charges, are not satisfied with the bonding of a 10-vertex *closo*-type cluster according to PSEPT theory (CVEs = 14 × 3 + 4 × 7 + 2 =

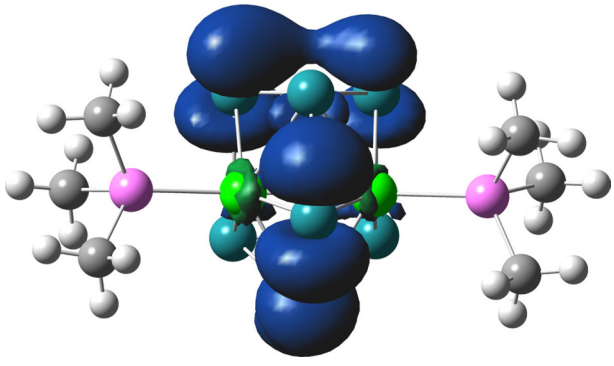

Figure 5 The spin density of cluster $\{Sb_7[Rh(PMe_3)]_2\}^{2-}$ (isovalue = 0.001).

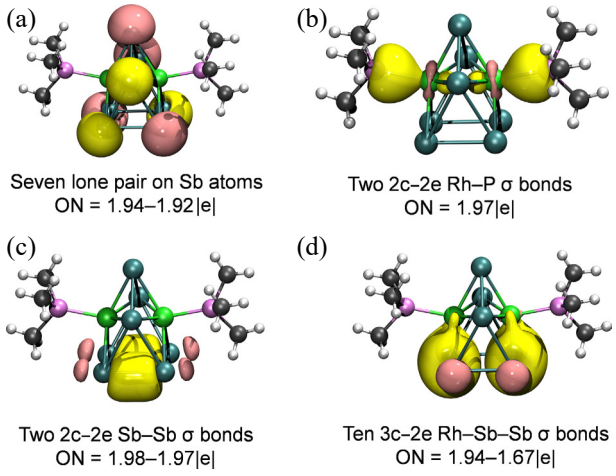

Figure 6 AdNDP analysis of the Sb_7Rh_2 nine-atom cage in cluster $\{Sb_7[Rh(PMe_3)]_2\}^{2-}$.

72). The AdNDP analysis of cluster $\{Sb_7[Rh(PMe_3)]_3\}^{2-}$ revealed that 142 valence electrons can be partitioned into the following classes except for the d-type lone pairs on Rh atoms and classical 2c–2e bonds in three PMe_3 units (with four 1c–2e bonds on each Rh atom, twenty-seven 2c–2e C–H bonds and nine P–C bonds, with ONs of 1.95–1.79|e|, 1.99|e|, and 1.98|e|, respectively) (Fig. S25 in the ESM). The first category is seven s-type lone pairs on each Sb atom with ON = 1.92–1.90|e| (Fig. 7(a)). The second class consists of three 2c–2e Rh–P bonds and three 2c–2e Sb–Sb bonds with occupation numbers of 1.98 and 1.84|e|, which is consistent with the linking-basal distances of Sb–Sb bonds in cluster $\{Sb_7[Rh(PMe_3)]_3\}^{2-}$ (Figs. 7(b) and 7(c)); the third class consists of nine 3c–2e Rh–Sb–Sb bonds, representing interactions of a Rh atom and the corresponding two basal Sb atoms (Fig. 7(d)) and interactions between a Rh atom, an apical Sb atom and the corresponding linking Sb atom (Fig. 7(e)). Finally, the remaining

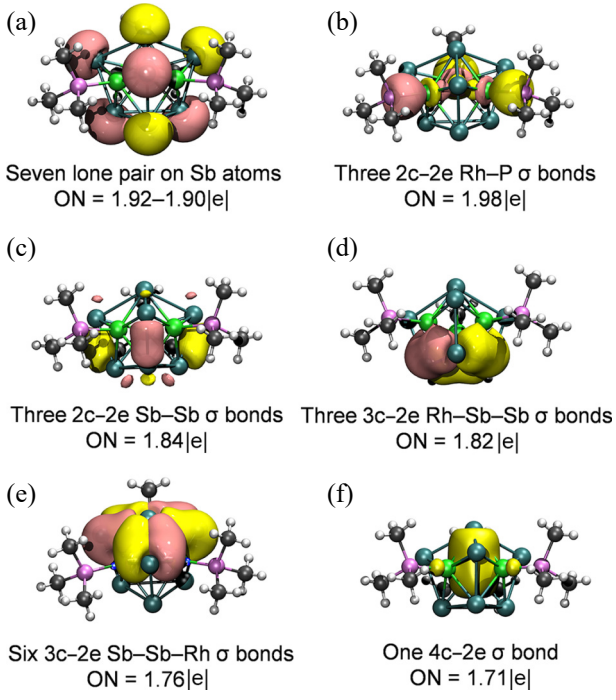

Figure 7 AdNDP analysis of the Sb_7Rh_3 ten-atom cage in cluster $\{Sb_7[Rh(PMe_3)]_3\}^{2-}$.

two electrons can be localized into a four-center–two-electron (4c–2e) Sb(apical)–Rh_3 bond (Fig. 7(f)). The contributions of three Rh atoms and one Sb atom to the formation of this bond are approximately 72.56% and 27.44%, respectively, which aligns with the weak interactions between the Rh atoms.

4 Conclusions

In summary, a series of novel Rh–Sb/Bi clusters **1**–**3**, constructed from the Pn_7 framework, PPh_3 unit, and/or Pn^- atoms, were successfully synthesized and isolated by subtle changes in the reaction conditions. These title clusters likely form through the assembly of a Pn_7^{3-} cage, followed by the addition of multi-metallic fragments to the polycyclic Pn_5 face within the Pn_7 framework. DFT calculations revealed weak 3c–2e $RhPn_2$ and Rh–Rh interactions, contributing to the stabilization of these clusters. Future work will concentrate on the controlled oxidation of these clusters to generate well-ordered bismuth-rich intermetallic nanoparticles, which have potential applications in catalysis and electrochemistry.

Electronic Supplementary Material: Supplementary material (crystallographic supplementary information, ESI-MS, EDS and computational details and results) is available in the online version of this article at https://doi.org/10.26599/NR.2025.94907253.

Data availability

All the data needed to support the conclusions in the paper are presented in the manuscript and the Electronic Supplementary Material. Additional data related to this paper may be requested from the corresponding author upon request.

Acknowledgements

This work was supported by the National Natural Science Foundation of China (Nos. 22425107, 92461303, 22371140, and 92161102 (Z.-M. S.)) and (No. 22301143 (L. Q.)).

Declaration of competing interest

All the contributing authors report no conflict of interests in this work.

Author contribution statement

L. Q.: Conceptualization, data curation, project administration, validation, writing manuscript, experimental design, funding acquisition. C.-L. C.: Writing – review & editing. Z.-M. S.: Conceptualization, funding acquisition, project administration, writing – review & editing, supervision. All the authors have approved the final manuscript.

Use of AI statement

None.

References

[1] Wang, Y.; McGrady, J. E.; Sun, Z. M. Solution-based group 14 Zintl anions: New frontiers and discoveries. *Acc. Chem. Res.* **2021**, *54*, 1506–1516.

[2] Mayer, K.; Weßing, J.; Fässler, T. F.; Fischer, R. A. Intermetalloid

clusters: Molecules and solids in a dialogue. *Angew. Chem., Int. Ed.* **2018**, *57*, 14372–14393.

[3] Qiao, L.; McGrady, J. E.; Sun, Z. M. Zintl chemistry: From Zintl ions to Zintl clusters. In *Comprehensive Inorganic Chemistry III*, 3rd ed.; Reedijk, J.; Poeppelmeier, K. R., Eds.; Elsevier: Amsterdam, 2023; pp 903–933.

[4] Pan, F. X.; Peerless, B.; Dehnen, S. Bismuth-based metal clusters-from molecular aesthetics to contemporary materials science. *Acc. Chem. Res.* **2023**, *56*, 1018–1030.

[5] Wilson, R. J.; Lichtenberger, N.; Weinert, B.; Dehnen, S. Intermetalloid and heterometallic clusters combining p-block (semi)metals with d- or f-block metals. *Chem. Rev.* **2019**, *119*, 8506–8554.

[6] Turbervill, R. S. P.; Goicoechea, J. M. From clusters to unorthodox pnictogen sources: Solution-phase reactivity of $[E_7]^{3-}$ (E = P–Sb) anions. *Chem. Rev.* **2014**, *114*, 10807–10828.

[7] van Ijzendoorn, B.; Mehta, M. Frontiers in the solution-phase chemistry of homoatomic group 15 Zintl clusters. *Dalton Trans.* **2020**, *49*, 14758–14765.

[8] Gärtner, S.; Korber, N. Zintl anions. In *Comprehensive Inorganic Chemistry II*, 2nd ed.; Reedijk, J.; Poeppelmeier, K., Eds.; Elsevier: Amsterdam, 2013; pp 251–267.

[9] Ahlrichs, R.; Fenske, D.; Fromm, K.; Krautscheid, H.; Krautscheid, U.; Treutler, O. Zintl anions as starting compounds for the synthesis of polynuclear transition metal complexes. *Chem.—Eur. J.* **1996**, *2*, 238–244.

[10] Knapp, C.; Zhou, B. B.; Denning, M. S.; Rees, N. H.; Goicoechea, J. M. Reactivity studies of group 15 Zintl ions towards homoleptic post-transition metal organometallics: A 'bottom-up' approach to bimetallic molecular clusters. *Dalton Trans.* **2010**, *39*, 426–436.

[11] Qian, M. C.; Reber, A. C.; Ugrinov, A.; Chaki, N. K.; Mandal, S.; Saavedra, H. M.; Khanna, S. N.; Sen, A.; Weiss, P. S. Cluster-assembled materials: Toward nanomaterials with precise control over properties. *ACS Nano* **2010**, *4*, 235–240.

[12] Mandal, S.; Reber, A. C.; Qian, M. C.; Liu, R.; Saavedra, H. M.; Sen, S.; Weiss, P. S.; Khanna, S. N.; Sen, A. Synthesis, structure and band gap energy of covalently linked cluster-assembled materials. *Dalton Trans.* **2012**, *41*, 12365–12377.

[13] Mandal, S.; Reber, A. C.; Qian, M. C.; Liu, R.; Saavedra, H. M.; Sen, S.; Weiss, P. S.; Khanna, S. N.; Sen, A. On the stability of an unsupported mercury-mercury bond linking group 15 Zintl clusters. *Dalton Trans.* **2012**, *41*, 5454–5457.

[14] Knapp, C. M.; Large, J. S.; Rees, N. H.; Goicoechea, J. M. A versatile salt-metathesis route to heteroatomic clusters derived from phosphorus and arsenic Zintl anions. *Dalton Trans.* **2011**, *40*, 735–745.

[15] Eichhorn, B. W.; Haushalter, R. C.; Huffman, J. C. Insertion of Cr $(CO)_3$ into $As_7^{3\ominus}$ to form $[As_7Cr(CO)]^{3\ominus}$: An inorganic nortricyclane-to-norbornadiene conversion. *Angew. Chem., Int. Ed.* **1989**, *28*, 1032–1033.

[16] Charles, S.; Eichhorn, B. W.; Rheingold, A. L.; Bott, S. G. Synthesis, structure, and properties of the $[E_7M(CO)_3]^{3-}$ complexes where E = P, As, Sb and M = Cr, Mo, W. *J. Am. Chem. Soc.* **1994**, *116*, 8077–8086.

[17] Bolle, U.; Tremel, W. Insertion of a transition metal fragment into a heptaantimonide(3−) anion: Synthesis and structure of $[Sb_7Mo(CO)_3]^{3-}$. *J. Chem. Soc., Chem. Commun.* **1994**, 217–219.

[18] Li, Z.; Ouyang, D.; Xu, L. $[Bi_7M_3(CO)_3]^{2-}$ (M = Co, Rh): A new architype of 10-vertex deltahedral hybrids by the unprecedented polycyclic η^5-coordination addition of Bi_7^{3-} and trimetallic fragments. *Chem. Commun.* **2019**, *55*, 6783–6786.

[19] Gascoin, F.; Sevov, S. C. Synthesis and characterization of the "metallic salts" A_5Pn_4 (A = K, Rb, Cs and Pn = As, Sb, Bi) with isolated zigzag tetramers of Pn_4^{4-} and an extra delocalized electron. *Inorg. Chem.* **2001**, *40*, 5177–5181.

[20] Osborn, J. A.; Jardine, F. H.; Young, J. F.; Wilkinson, G. The preparation and properties of tris(triphenylphosphine)halogenorhodium(I) and some reactions thereof including catalytic homogeneous hydrogenation of olefins and acetylenes and their derivatives. *J. Chem. Soc. A* **1966**, 1711–1732.

[21] Wakatsuki, Y.; Yamazaki, H. Some reactions of π-cyclopentadienylbis(triphenylphosphine) rhodium(I). *J. Organomet. Chem.* **1974**, *64*, 393–402.

[22] Sheldrick, G. M. *SHELXT*-integrated space-group and crystal-structure determination. *Acta Crystallogr. Sect. A: Found. Adv.* **2015**, *71*, 3–8.

[23] Dolomanov, O. V.; Bourhis, L. J.; Gildea, R. J.; Howard, J. A. K.; Puschmann, H. *OLEX2*: A complete structure solution, refinement and analysis program. *J. Appl. Crystallogr.* **2009**, *42*, 339–341.

[24] Spek, A. L. Structure validation in chemical crystallography. *Acta Crystallogr. Sect. D: Biol. Crystallogr.* **2009**, *65*, 148–155.

[25] Frisch, M. J.; Trucks, G. W.; Schlegel, H. B.; Scuseria, G. E.; Robb, M. A.; Cheeseman, J. R.; Scalmani, G.; Barone, V.; Mennucci, B.; Petersson, G. A. et al. *Gaussian 09*, Revision D. 01; Gaussian, Inc.: Wallingford, CT, USA, 2013.

[26] Adamo, C.; Barone, V. Toward reliable density functional methods without adjustable parameters: The PBE0 model. *J. Chem. Phys.* **1999**, *110*, 6158–6170.

[27] Zubarev, D. Y.; Boldyrev, A. I. Developing paradigms of chemical bonding: Adaptive natural density partitioning. *Phys. Chem. Chem. Phys.* **2008**, *10*, 5207–5217.

[28] Lu, T.; Chen, F. W. Multiwfn: A multifunctional wavefunction analyzer. *J. Comput. Chem.* **2012**, *33*, 580–592.

[29] Perla, L. G.; Oliver, A. G.; Sevov, S. C. Bi_7^{3-}: The missing family member, finally isolated and characterized. *Inorg. Chem.* **2015**, *54*, 872–875.

[30] Xu, L.; Ugrinov, A.; Sevov, S. C. Stabilization of ozone-like $[Bi_3]^{3-}$ in the heteroatomic *closo*-clusters $[Bi_3Cr_2(CO)_6]^{3-}$ and $[Bi_3Mo_2(CO)_6]^{3-}$. *J. Am. Chem. Soc.* **2001**, *123*, 4091–4092.

[31] Goicoechea, J. M.; Hull, M. W.; Sevov, S. C. Heteroatomic deltahedral clusters: Synthesis and structures of *closo*-$[Bi_3Ni_4(CO)_6]^{3-}$, *closo*-$[Bi_4Ni_4(CO)_6]^{2-}$, the open cluster $[Bi_3Ni_6(CO)_9]^{3-}$, and the Intermetalloid *closo*-$[Ni_x@\{Bi_6Ni_6(CO)_8\}]^{4-}$. *J. Am. Chem. Soc.* **2007**, *129*, 7885–7893.

[32] Qiao, L.; Yang, T.; Frenking, G.; Sun, Z. M. $[Ga@Bi_{10}(NbMes)_2]^{3-}$: A linear Nb–$Ga^{I}$–Nb filament coordinated by a bismuth cage. *Chem. Commun.* **2023**, *59*, 4024–4027.

[33] Qiao, L.; Chen, D. D.; Zhu, J.; Muñoz-Castroc, A.; Sun, Z. M. $[Bi_6Mo_3(CO)_9]^{4-}$: A multiple local σ-aromatic cluster containing a distorted Bi_6 triangular prism. *Chem. Commun.* **2021**, *57*, 3656–3659.

[34] Lichtenberger, N.; Spang, N.; Eichhöfer, A.; Dehnen, S. Between localization and delocalization: $Ru(cod)^{2+}$ units in the Zintl clusters $[Bi_9\{Ru(cod)\}_2]^{3-}$ and $[Tl_2Bi_6\{Ru(cod)\}]^{2-}$. *Angew. Chem., Int. Ed.* **2017**, *56*, 13253–13258.

[35] Femoni, C.; Bussoli, G.; Ciabatti, I.; Ermini, M.; Hayatifar, M.; Iapalucci, M. C.; Ruggieri, S.; Zacchini, S. Interstitial bismuth atoms in icosahedral rhodium cages: Syntheses, characterizations, and molecular structures of the $[Bi@Rh_{12}(CO)_{27}]^{3-}$, $[(Bi@Rh_{12}(CO)_{26})_2Bi]^{5-}$, $[Bi@Rh_{14}(CO)_{27}Bi_2]^{3-}$, and $[Bi@Rh_{17}(CO)_{33}Bi_2]^{4-}$ carbonyl clusters. *Inorg. Chem.* **2017**, *56*, 6343–6351.

[36] Slater, J. C. Atomic radii in crystals. *J. Chem. Phys.* **1964**, *41*, 3199–3204.

[37] Charles, S.; Eichhorn, B. W.; Bott, S. G. Synthesis and structure of $[Sb_7Ni_3(CO)_3]^{3-}$: A new structural type for nido 10-vertex polyhedral clusters. *J. Am. Chem. Soc.* **1993**, *115*, 5837–5838.

[38] Critchlow, S. C.; Corbett, J. D. Homopolyatomic anions of the post transition elements. Synthesis and structure of potassium-crypt salts of the tetraantimonide(2−) and heptaantimonide(3−) anions, Sb_4^{2-} and Sb_7^{3-}. *Inorg. Chem.* **1984**, *23*, 770–774.

[39] Adolphson, D. G.; Corbett, J. D.; Merryman, D. J. Stable homopolyatomic anions of the post-transition metals. "Zintl ions".

The synthesis and structure of a salt containing the heptantimonide(3−) anion. *J. Am. Chem. Soc.* **1976**, *98*, 7234–7239.

[40] Femoni, C.; Funaioli, T.; Iapalucci, C. M.; Ruggieri, S.; Zacchini, S. Rh–Sb nanoclusters: Synthesis, structure, and electrochemical studies of the atomically precise $[Rh_{20}Sb_3(CO)_{36}]^{3-}$ and $[Rh_{21}Sb_2(CO)_{38}]^{5-}$ carbonyl compounds. *Inorg. Chem.* **2020**, *59*, 4300–4310.

[41] Bolle, U.; Tremel. W. $[Na(2,2,2,\text{-crypt})]_3[Sb_{11}]$, a salt containing the undecaantimonide(3−) anion. *J. Chem. Soc., Chem. Commun.* **1992**, 91–93.

[42] Zhai, J.; Xu, L. Synthesis and crystal structure of $[K(2,2,2\text{-crypt})]_3Sb_{11}$. *Chin. J. Struct. Chem.* **2011**, *30*, 1091–1094.

[43] Mingos, D. M. P. A general theory for cluster and ring compounds of the main group and transition elements. *Nat. Phys. Sci.* **1972**, *236*, 99–102.

[44] Wade, K. The structural significance of the number of skeletal bonding electron-pairs in carboranes, the higher boranes and borane anions, and various transition-metal carbonyl cluster compounds. *J. Chem. Soc. D* **1971**, 792–793.

[45] Mingos, D. M. P. Polyhedral skeletal electron pair approach. *Acc. Chem. Res.* **1984**, *17*, 311–319.

[46] Zhang, W. Q.; Tkachenko, N. V.; Qiao, L.; Boldyrev, A. I.; Sun, Z. M. Synthesis and structure of binary copper/silver-arsenic clusters derived from Zintl ion As_7^{3-}. *Chin. J. Chem.* **2022**, *40*, 65–70.

[47] Chen, W. X.; Tkachenko, N. V.; Muñoz-Castro, A.; Boldyrev, A. I.; Sun, Z. M. Ruthenium-mediated assembly and enhanced stability of heterometallic polystannides $[Ru_2Sn_{19}]^{4-}$ and $[Ru_2Sn_{20}]^{6-}$. *Nano Res.* **2022**, *15*, 5705–5711.

[48] Popov, I. A.; Pan, F. X.; You, X. R.; Li, L. J.; Matito, E.; Liu, C.; Zhai, H. J.; Sun, Z. M.; Boldyrev, A. I. Peculiar all-metal σ-aromaticity of the $[Au_2Sb_{16}]^{4-}$ anion in the solid state. *Angew. Chem., Int. Ed.* **2016**, *55*, 15344–15346.

[49] Qiao, L.; Zhang, C.; Shu, C. C.; Morgan, H. W. T.; McGrady, J. E.; Sun, Z. M. $[Cu_4@E_{18}]^{4-}$ (E = Sn, Pb): Fused derivatives of endohedral stannaspherene and plumbaspherene. *J. Am. Chem. Soc.* **2020**, *142*, 13288–13293.

[50] Liu, C.; Tkachenko, N. V.; Popov, I. A.; Fedik, N.; Min, X.; Xu, C. Q.; Li, J.; McGrady, J. E.; Boldyrev, A. I.; Sun, Z. M. Structure and bonding in $[Sb@In_8Sb_{12}]^{3-}$ and $[Sb@In_8Sb_{12}]^{5-}$. *Angew. Chem., Int. Ed.* **2019**, *58*, 8367–8371.